

2D watershed void clustering for probing the cosmic large-scale structure

YINGXIAO SONG,^{1,2} YAN GONG*,^{1,2} QI XIONG,^{1,2} KWAN CHUEN CHAN,^{3,4} XUELEI CHEN,^{1,2,5,6} QI GUO,^{1,2} YUN LIU,^{1,2} AND WENXIANG PEI^{1,2}

¹*National Astronomical Observatories, Chinese Academy of Sciences, 20A Datun Road, Beijing 100012, China*

²*University of Chinese Academy of Sciences(UCAS), Beijing 100049, China*

³*School of Physics and Astronomy, Sun Yat-sen University, 2 Daxue Road, Tangjia, Zhuhai, 519082, China*

⁴*CSSST Science Center for the Guangdong-Hongkong-Macau Greater Bay Area, SYSU, Zhuhai, 519082, China*

⁵*Department of Physics, College of Sciences, Northeastern University, Shenyang 110819, China*

⁶*Centre for High Energy Physics, Peking University, Beijing 100871, China*

ABSTRACT

Cosmic void has been proven to be an effective cosmological probe of the large-scale structure (LSS). However, since voids are usually identified in spectroscopic galaxy surveys, they are generally limited to low number density and redshift. We propose to utilize the clustering of two-dimensional (2D) voids identified using Voronoi tessellation and watershed algorithm without any shape assumption to explore the LSS. We generate mock galaxy and void catalogs for the next-generation Stage IV photometric surveys in $z = 0.8 - 2.0$ from simulations, develop the 2D void identification method, and construct the theoretical model to fit the 2D watershed void and galaxy angular power spectra. We find that our method can accurately extract the cosmological information, and the constraint accuracies of some cosmological parameters from the 2D watershed void clustering are even comparable to the galaxy angular clustering case, which can be further improved by as large as $\sim 30\%$ in the void and galaxy joint constraints. This indicates that the 2D void clustering is a good complement to galaxy angular clustering measurements, especially for the forthcoming Stage IV surveys that detect high-redshift universe.

Keywords: Voids (1779), Cosmological parameters (339), Large-scale structure of the universe (902)

1. INTRODUCTION

Cosmic voids are the regions with low densities and large volumes in the large-scale structure (LSS) of the Universe. It can be an effective cosmological probe for exploring the LSS (e.g. Chan & Hamaus 2021; Schuster et al. 2023; Mauland et al. 2023). In particular, the three dimensional (3D) voids have been widely used in the studies of the LSS based on the statistical properties, such as void size function and number counts (Contarini et al. 2021, 2022, 2023; Pellicciari et al. 2023; Verza et al. 2024; Song et al. 2024a,b). However, since 3D voids are generally identified in spectroscopic surveys, they have some limitations or disadvantages in the LSS study, e.g. low number densities with poor statistics and locating at low redshifts with small redshift coverage. On the

other hand, if we can properly identify 2D voids in photometric surveys and correctly model them, the usability of voids as a cosmological probe can be greatly improved. Although some attempts have been made to use the 2D voids for exploring the LSS (e.g. Sánchez et al. 2017; Cautun et al. 2018; Vielzeuf et al. 2021; Bonici et al. 2023; Vielzeuf et al. 2023; Camacho-Ciurana et al. 2023), they are still preliminary which assume spherical void shapes and relatively simple modeling.

In this work, we propose a 2D void identification method based on the Voronoi tessellation (e.g. van de Weygaert & Schaap 2009) and watershed algorithm (Platen et al. 2007) without any shape assumption, and develop the corresponding theoretical model of the 2D watershed void clustering power spectrum using the halo model (Hamaus et al. 2014b). The identification algorithm can find low surface density regions with natural and non-spherical shapes, and provide excellent 2D void clustering information for cosmological studies. This

method can be applied to the next-generation Stage IV galaxy surveys, such as the Legacy Survey of Space and Time (LSST) (Ivezić et al. 2019), *Euclid* (Euclid Collaboration et al. 2022), Roman space telescopes (RST) (Akeson et al. 2019), and the China Space Station Telescope (CSST) (Zhan 2011, 2021; Gong et al. 2019; Miao et al. 2023).

Taking the CSST photometric galaxy survey as an example, we generate the mock galaxy and void catalogs based on simulations and the CSST survey strategy. Then we derive the mock data of the void and galaxy auto and cross angular power spectra in four tomographic photometric redshift (photo- z) bins from $z = 0.8$ to 2.0. The Markov Chain Monte Carlo (MCMC) method is employed to constrain the cosmological and void parameters for exploring the feasibility and effectiveness of our method.

The Letter is organized as follows: In Section 2, we introduce the mock galaxy and 2D watershed void catalogs we use; In Section 3, we discuss the calculation of the theoretical model and generation of the mock data for the 2D void and galaxy clustering; In Section 4, we show the constraint results; We give our conclusion in Section 5.

2. MOCK CATALOGS

We generate the mock galaxy and 2D void catalogs from the dark matter-only Jiutian simulation, which contains 6144^3 particles with a mass resolution of $m_p = 3.72 \times 10^8 h^{-1} M_\odot$ and box size $1 h^{-1} \text{Gpc}$. The fiducial cosmology we set are from *Planck*2018, i.e. $h = 0.6766$, $\Omega_m = 0.3111$, $\Omega_b = 0.0490$, $\Omega_\Lambda = 0.6899$, $\sigma_8 = 0.8102$ and $n_s = 0.9665$ (Planck Collaboration et al. 2020). The friend-of-friend and subfind algorithm are used to identify dark matter halos and substructures (Springel et al. 2001; Springel 2005). We use an updated version of the L-Galaxies semi-analytical model to place galaxies and construct a light cone covering 100 deg^2 sky area from $z = 0$ to 3 (Springel 2005; Croton et al. 2006; De Lucia & Blaizot 2007; Guo et al. 2011; Henriques et al. 2015; Pei et al. 2024). By tracking the merger tree of each galaxy, we can consider the evolution effect and naturally avoid galaxy repetition or omission at the boundary of slices. Galaxies are selected based on the apparent magnitude limits of the CSST photometric survey, which can reach $i \sim 26$ AB mag for 5σ point source detection (Gong et al. 2019).

Since the LSS at low redshifts can be well measured by spectroscopic surveys, here we mainly focus on the high redshifts at $z > 0.8$. We also note that the galaxy density decreases quickly at $z > 2$ in the CSST photometric survey (Gong et al. 2019), which can dramati-

cally suppress the surface density of 2D voids. Hence we only consider the redshift range $z = 0.8 - 2.0$ in our analysis, and split the galaxy sample into four photo- z tomographic bins to extract more information and reduce 2D void overlapping effect. In Table 1, we show the galaxy surface densities n_g and redshift ranges for the four photo- z bins we consider. The redshift range for each bin is determined to make n_g similar in each bin.

We implement the Voronoi tessellation and watershed algorithm to identify 2D voids in our mock galaxy catalog (Virtanen et al. 2020; Kenneth E. Bellock. 2019; OpenCV 2015). The Voronoi tessellation allocates a cell to each galaxy based on the principle that each cell contains the region of space with a shorter distance to a galaxy than the distance to the galaxies in the other cells. The purpose of the Voronoi cells is to estimate the density field, and the size of each cell reflects the difference in density. The density of a cell is derived by $\rho_{\text{cell}} = 1/S_{\text{cell}}$, and S_{cell} is the area of the cell. And the watershed algorithm performs the process of merging Voronoi cells. Starting at the minimum density, adjacent cells with increasing density are combined to form the zone. The zone stops growing when the densities of all adjacent cells are greater than $\bar{\rho} = \sum \rho_{\text{cell}}/N_{\text{cell}}$ to form the 2D watershed void in our mock void catalog, where N_{cell} is the number of cells.

The void angular radius θ_v is calculated from an effective circle with an area S_v equal to the total area of all cells within the void. Then the void area-weighted center \mathbf{X}_v also can be estimated using the positions of the cells, and we have

$$S_v = \sum_i S_{\text{cell}}^i = \pi \theta_v^2, \quad \text{and} \quad \mathbf{X}_v = \frac{1}{S_v} \sum_i \mathbf{x}_i S_{\text{cell}}^i. \quad (1)$$

Here S_{cell}^i represents the area of the cell i , and \mathbf{x}_i is the coordinate of the galaxy within a cell in a given void. Note that there is one parameter, which is called the cut distance D_{cut} , in our 2D void finder that determines whether to finish the process of zone merging growth to a void. D_{cut} is derived based on the distance from a pixel point inside a void to the void boundary, and is normalized based on the maximum D_{cut} in the map, which takes the values from 0 to 1. Then we discard the cells in a void candidate with D_{cut} for the galaxy in a cell less than a certain value to trim the void. The smaller the value of D_{cut} we choose, the larger the size of a void we retain.

In Figure 1, as an example, we show the effects of identifying 2D watershed voids by selecting different D_{cut} values. We can find that the identified 2D void (red regions) and the effective angular radius θ_v (red circle)

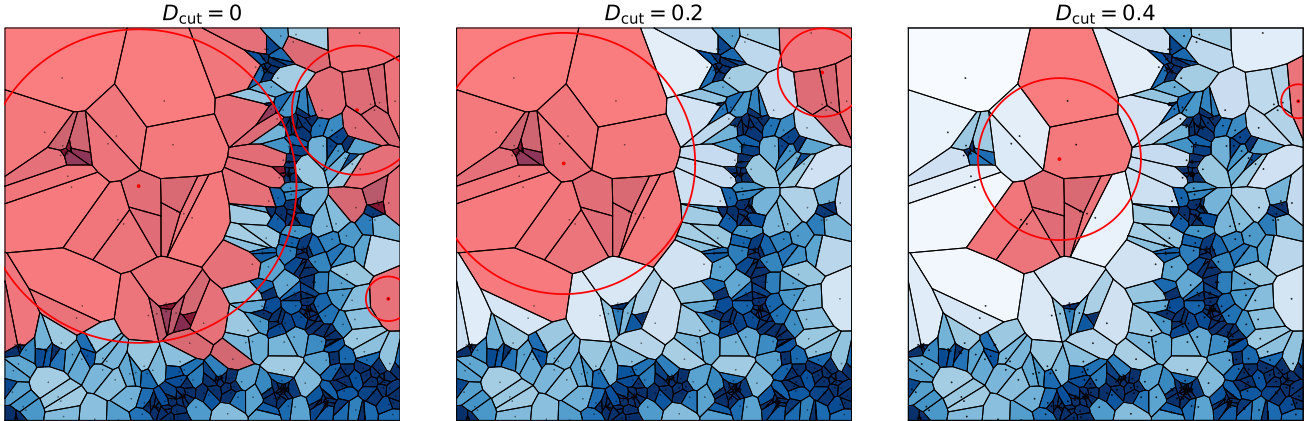


Figure 1. The voids identified by choosing $D_{\text{cut}} = 0$ (left), 0.2 (middle), and 0.4 (right). The density of each cell is shown in red or blue, and darker colors indicate higher densities. The 2D watershed voids are shown as red regions, and the red circles and dots denote the effective angular radius θ_v and area-weighted centers \mathbf{X}_v , respectively.

Table 1. The galaxy and void surface number densities, i.e. n_g and n_v (in arcmin^{-2}), in the four photo- z tomographic bins from $z = 0.8$ to 2.0. The mean, minimum and maximum angular radii of voids θ_v (in arcsec) with $R_v > 1 h^{-1}\text{Mpc}$ and $D_{\text{cut}} = 0.2$ are also shown.

z_{min}	z_{max}	n_g	n_v	θ_v^{mean}	θ_v^{min}	θ_v^{max}
0.8	1.0	3.59	0.0025	5.4	1.7	75.6
1.0	1.2	2.86	0.0022	3.9	1.5	32.5
1.2	1.5	3.08	0.0023	3.3	1.3	22.7
1.5	2.0	3.51	0.0049	2.9	1.1	26.8

are well matched when $D_{\text{cut}} = 0.2$, which means that θ_v and \mathbf{X}_v are calculated more accurately in this case. So we choose $D_{\text{cut}} = 0.2$ as our default value for identifying 2D voids in the analysis. Besides, to reduce the non-linear evolution effect and the incompleteness of the small-size voids, we remove the voids with the effective radius $R_v = \theta_v D_A < 1 h^{-1}\text{Mpc}$, where D_A is the comoving angular diameter distance. In Table 1, we show the 2D void surface number densities, and the average, minimum and maximum angular radii of 2D voids with $D_{\text{cut}} = 0.2$ and $R_v > 1 h^{-1}\text{Mpc}$ in the four photo- z tomographic bins. We find that the mean void angular radius θ_v^{mean} has a trend to become smaller as redshift increases, while the mean void radius R_v^{mean} is similar ($\sim 3 h^{-1}\text{Mpc}$) at $z < 2$.

3. ANGULAR POWER SPECTRUM

We model the galaxy and void auto and cross angular power spectrum based on the halo model (Hamaus

et al. 2014b). Assuming Limber approximation (Limber 1954), the galaxy and void angular power spectra can be written as

$$C_{\text{AB}}^{ij}(\ell) = \frac{1}{c} \int \frac{H(z)}{D_A^2(z)} W_A^i(z) W_B^j(z) P_{\text{mm}} \left[\frac{\ell + 1/2}{D_A(z)}, z \right] dz, \quad (2)$$

where A and B denote two different tracers, c is the speed of light, and P_{mm} is the matter power spectrum, where the wavenumber k is converted by the multipole ℓ and comoving angular diameter distance D_A . In this work, we use CAMB (Lewis et al. 2000) to calculate P_{mm} and D_A .

The galaxy weighting function is given by $W_g^i(z) = b_g^i n_g^i(z)$, where b_g^i is the galaxy bias, and $n_g^i(z)$ is the normalized galaxy redshift distribution in the i th bin. For the void weighting function, we include the void density profile in the model and find that

$$W_v^i(z) = b_v^i n_v^i(z) u_v^i \left[k = \frac{\ell + 1/2}{D_A(z)}, z \right]. \quad (3)$$

Here b_v^i is the void bias, and $n_v^i(z)$ is the normalized void redshift distribution in the i th bin. $u_v(k)$ is the normalized void density profile in Fourier space (Hamaus et al. 2014b)

$$u_v(k) = \frac{\bar{\rho}}{\delta m} \int_{R_v^{\text{min}}}^{R_v^{\text{max}}} u_v(r) \frac{\sin(kr)}{kr} 4\pi r^2 dr. \quad (4)$$

Here δm is the void uncompensated mass, which is given by $\delta m = \bar{\rho} \int_{R_v^{\text{min}}}^{R_v^{\text{max}}} u_v(r) 4\pi r^2 dr$, and $u_v(r)$ is the averaged spherically deviation between the void mass density and the mean matter density of the entire universe. It can be derived from the form in the real space (Hamaus et al. 2014a)

$$u_v(r) = \frac{\rho_v(r)}{\bar{\rho}} - 1 = \delta_{\text{cen}} \frac{1 - (r/R_s)^\alpha}{1 + (r/R_v)^\beta}. \quad (5)$$

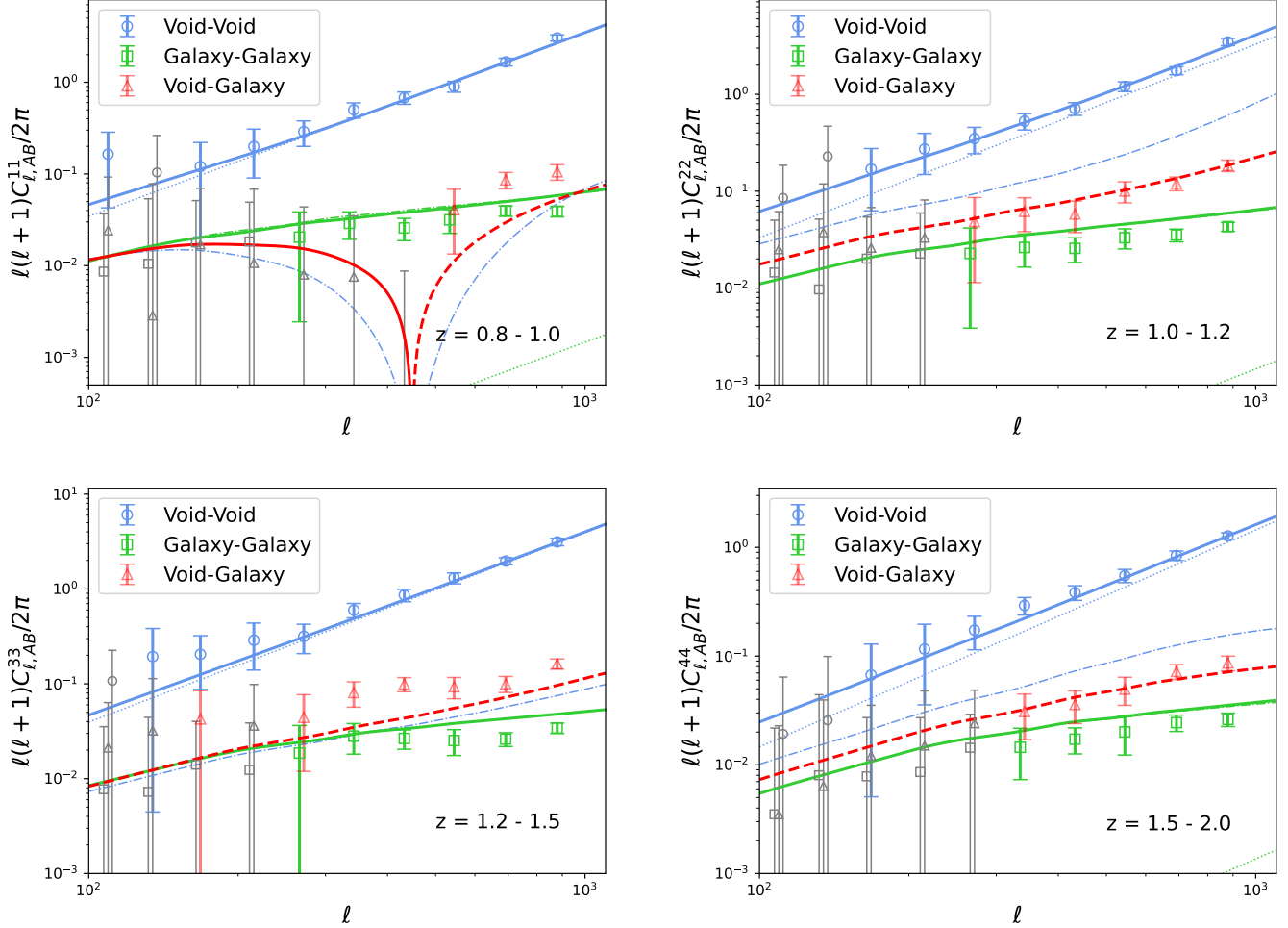


Figure 2. The angular power spectra C_{vv}^{ij} (blue), C_{gg}^{ij} (green) and C_{vg}^{ij} (red) with $i = j$ in the four redshift tomographic bins from the 100 deg^2 simulation. The gray data points with $\text{SNR} < 1$ are excluded from the constraint process. The curves are the best-fits of the theoretical calculation. The red dashed lines and data points indicate that the values are negative. The solid (or dashed), dash-dotted and dotted curves are the total, clustering and noise terms of the power spectra, respectively.

Here $R_s \equiv \gamma R_v$ is the scale radius when the void density $\rho_v = \bar{\rho}$, where γ is the ratio factor and $\bar{\rho}$ is the mean matter density. $\delta_{\text{cen}} = -1$ is the central density contrast, which can be cancelled out in our analysis (see Eq. (4)). α and β denote the inner and outer slopes of the compensation wall around a void, and we set them as free parameters in our fitting process. Here we propose to simplify the calculation by setting $R_v = R_v^{\text{mean}}$ in Eq. (5). This means that $u_v(r)$ and $u_v(k)$, as well as R_s , α , β and γ , are the mean values of all voids selected in a redshift bin.

When we calculate the angular power spectra of galaxy, void and galaxy-void, statistical and systematic uncertainties are also considered by adding the noise term $\tilde{C}_{\text{AB}} = C_{\text{AB}} + N_{\text{AB}}$, where N_{AB} contains the shot noise and systematics. Besides the three parameters from the void density profile, we also set the galaxy

bias b_g , void bias b_v , and noise terms as free parameters when constraining the cosmological parameters.

We use `powerbox` (Murray 2018) to derive the data of the void and galaxy angular power spectra from the mock catalogs, and estimate errors using the jackknife method. We only use the data points with the signal-to-noise ratio (SNR) > 1 to obtain sufficient statistical significance in the fitting process. In Figure 2, we show the mock data of the galaxy, void and void-galaxy angular power spectra at four redshift bins in the 100 deg^2 survey area from the simulation. Note that we only consider the void and galaxy angular power spectra in the same redshift bin for simplicity, since the cross power spectra between different photo- z bins are relatively small with large errors, especially for voids. In the full Stage IV surveys with more than ten thousand survey area, these cross power spectra need to be considered.

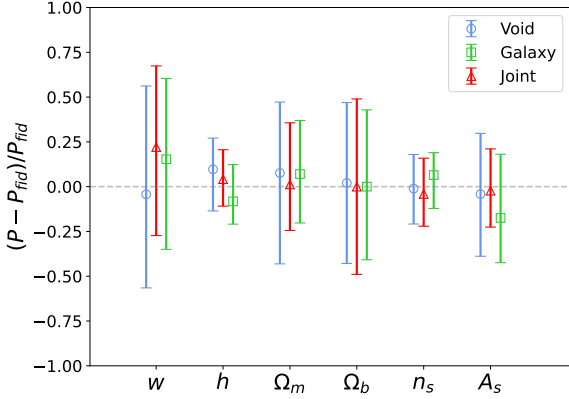


Figure 3. The residuals between the best-fit and fiducial values of the cosmological parameters from the simulation covering 100 deg^2 . The error bars denote the 1σ constraint results.

4. PARAMETER CONSTRAINT

We constrain the model parameters using χ^2 method, and the likelihood function can be derived by $\mathcal{L} \propto \exp(-\chi^2/2)$. The total χ^2 for the joint constraints with all power spectra in the four redshift bins can be calculated by $\chi_{\text{tot}}^2 = \chi_{\text{vv}}^2 + \chi_{\text{gg}}^2 + \chi_{\text{vg}}^2$, where χ_{vv}^2 , χ_{gg}^2 and χ_{vg}^2 are the chi-squares for the void, galaxy and void-galaxy angular power spectrum. The MCMC is employed to constrain the free parameters, which is performed by **emcee** (Foreman-Mackey et al. 2013) code. We choose 112 walkers and obtain 30000 steps for each chain. The first 10 percent of steps are discarded as the burn-in process.

In the parameter constraint process, we assume flat priors, and have included 6 cosmological parameters, i.e. $w \in (-1.8, -0.2)$, $h \in (0.5, 0.9)$, $\Omega_m \in (0.1, 0.5)$, $\Omega_b \in (0.02, 0.08)$, $A_s/10^{-9} \in (1, 3)$, $n_s \in (0.7, 1.2)$, and 3 void parameters $\alpha^i \in (0, 10)$, $\beta^i \in (0, 20)$, $\gamma^i \in (0, 2)$ in each redshift bin. The galaxy and void biases $b_g^i \in (0, 5)$ and $b_v^i \in (-20, 20)$, and noise terms $\log_{10}(N_g^i) \in (-20, 0)$, $\log_{10}(N_v^i) \in (-20, 0)$ and $N_{\text{vg}}^i/10^{-8} \in (-1000, 1000)$ in each redshift bin are also considered. Note that N_{vg} can have both positive and negative values since it contains the statistical uncertainty from measuring the void density profile (Hamaus et al. 2014b). We also consider the 1σ constraint results from the galaxy angular power spectra only, and set tighter prior ranges for b_g^i to obtain better constraint results in the joint fitting case.

The best-fit curves of the theoretical model in the fourth redshift bin are shown in Figure 2. We can find that the theoretical curves can fit the 2D watershed void, galaxy and void-galaxy power spectra well. In Figure 3, we show the residuals between the best-fit and fiducial values. We can see that the fitting results of the cosmological parameters are consistent with the fiducial values

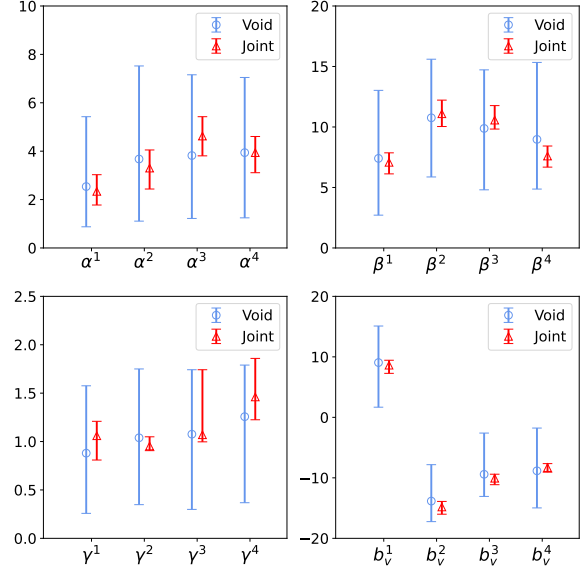


Figure 4. The best-fit and 1σ constraint results of α^i , β^i , γ^i and b_v^i from the void only (blue) and joint constraints (red).

within 1σ confidence level (CL). These indicate that our 2D void identification method can effectively produce the 2D void catalog, and our theoretical model can accurately extract the cosmological information from the 2D watershed void clustering.

We also notice that although the noise term is large in the 2D void power spectrum mainly due to the relatively low surface number density, the constraint powers for some cosmological parameters, e.g. h and A_s , are comparable to the galaxy angular power spectrum, and w and n_s are only slightly worse. Besides, the constraint accuracy can be further improved as large as $\sim 30\%$ in the joint constraint case, compared to the galaxy only case. This indicates that the 2D watershed void clustering can complement the galaxy clustering measurement for extracting cosmological information as an effective cosmological probe.

In Figure 4, we show the best-fits and 1σ CL of α , β , γ and b_v from the void power spectrum only and joint constraints. We can find that the constraint results are consistent within 1σ for these two cases, and the results from the joint constraints improve significantly by considering the galaxy and void-galaxy power spectra. We also notice that the best-fit values of α^i , β^i and γ^i have no obvious evolution trend with redshift, and basically fluctuate around certain values, i.e. $\alpha \sim 3.5$, $\beta \sim 9$ and $\gamma \sim 1$. For the void bias b_v , the best-fit value is positive in the first redshift bin with $z < 1$, and negative at $z > 1$. And we note that the probability distributions of b_v can cover both positive and negative values when only considering the 2D void power spectrum. And the joint

constraints can further improve the accuracy by about several times or even one order of magnitude on b_v^i and as large as 80% on α^i , β^i and γ^i . These results are also consistent with the previous 3D void studies (e.g. Fang et al. 2019; Song et al. 2024c).

In addition, the other systematical parameters, such as b_g , N_g , N_v and N_{vg} , are also well constrained in our analysis. We obtain $b_g^1 = 1.560_{-0.181}^{+0.227}$, $b_g^2 = 1.724_{-0.192}^{+0.257}$, $b_g^3 = 2.095_{-0.265}^{+0.257}$, $b_g^4 = 2.480_{-0.217}^{+0.333}$ in the joint fitting process. For the noise term of the void and galaxy angular power spectrum, we have similar constraint results as $\log_{10}(N_v^i) \simeq -5$ and $\log_{10}(N_g^i) \simeq -8$ at i th redshift bins, which give the constraint accuracies as $\log_{10}(N_v^i) \sim 1\%$ and $\log_{10}(N_g^i) \sim 10\%$ in the joint fitting process. And we have the constraint results of the noise from void-galaxy angular power spectrum as $N_{vg}^1/10^{-8} = -0.594_{-1.188}^{+1.380}$, $N_{vg}^2/10^{-8} = 1.187_{-0.886}^{+1.078}$, $N_{vg}^3/10^{-8} = -29.733_{-0.999}^{+0.982}$, $N_{vg}^4/10^{-8} = 0.546_{-1.475}^{+1.070}$ in the joint fitting process. We find that the joint constraints can provide a $\sim 50\%$ improvement on b_g^i and $\sim 70\%$ on N_g^i at i th redshift bins. Since the noise term N_v is dominated in measuring the void angular power spectrum, we can obtain tight constraint on N_v from both void angular power spectrum only and joint constraint, which are consistent within 1σ .

5. CONCLUSION

We propose to use the clustering of 2D watershed voids with natural and non-spherical shapes to explore the LSS. We develop a 2D void identification method based on the Voronoi tessellation and watershed algorithm, and build a theoretical model to extract the cosmological and void information. By generating the galaxy and void mock catalog using Jiutian simulations

for the CSST photometric survey covering 100 deg^2 from $z = 0.8 - 2.0$, we study the feasibility of this method.

We find that the watershed void and void-galaxy angular power spectrum can accurately derive the cosmological information, and the best-fit values of the cosmological parameters are consistent with the fiducial values within 1σ CL. The constraint strength of 2D void clustering for some cosmological parameters is comparable to the galaxy angular clustering, and the constraint accuracy can be improved as large as $\sim 30\%$ in the joint fitting case. These indicate that the 2D watershed void clustering can be an effective cosmological probe and a good complement to the galaxy photometric survey, especially for the upcoming Stage IV surveys to probe the high- z universe.

YS and YG acknowledge the support from National Key R&D Program of China grant Nos. 2022YFF0503404, 2020SKA0110402, and the CAS Project for Young Scientists in Basic Research (No. YSBR-092). KCC acknowledges the support the National Science Foundation of China under the grant number 12273121. XLC acknowledges the support of the National Natural Science Foundation of China through Grant Nos. 11473044 and 11973047, and the Chinese Academy of Science grants ZDKYYQ20200008, QYZDJ-SSW-SLH017, XDB 23040100, and XDA15020200. QG acknowledges the support from the National Natural Science Foundation of China (NSFC No.12033008). This work is also supported by science research grants from the China Manned Space Project with Grant Nos. CMS-CSST-2021-B01 and CMS-CSST-2021-A01.

REFERENCES

- Akeson, R., Armus, L., Bachelet, E., et al. 2019, arXiv e-prints, arXiv:1902.05569, doi: [10.48550/arXiv.1902.05569](https://doi.org/10.48550/arXiv.1902.05569)
- Bonici, M., Carbone, C., Davini, S., et al. 2023, *A&A*, 670, A47, doi: [10.1051/0004-6361/202244445](https://doi.org/10.1051/0004-6361/202244445)
- Camacho-Ciurana, G., Lee, P., Arsenov, N., et al. 2023, arXiv e-prints, arXiv:2312.08483, doi: [10.48550/arXiv.2312.08483](https://doi.org/10.48550/arXiv.2312.08483)
- Cautun, M., et al. 2018, *MNRAS*, 476, 3195, doi: [10.1093/mnras/sty463](https://doi.org/10.1093/mnras/sty463)
- Chan, K. C., & Hamaus, N. 2021, *PhRvD*, 103, 043502, doi: [10.1103/PhysRevD.103.043502](https://doi.org/10.1103/PhysRevD.103.043502)
- Contarini, S., Marulli, F., Moscardini, L., et al. 2021, *MNRAS*, 504, 5021, doi: [10.1093/mnras/stab1112](https://doi.org/10.1093/mnras/stab1112)
- Contarini, S., Pisani, A., Hamaus, N., et al. 2023, *ApJ*, 953, 46, doi: [10.3847/1538-4357/acde54](https://doi.org/10.3847/1538-4357/acde54)
- Contarini, S., Verza, G., Pisani, A., et al. 2022, *A&A*, 667, A162, doi: [10.1051/0004-6361/202244095](https://doi.org/10.1051/0004-6361/202244095)
- Croton, D. J., Springel, V., White, S. D. M., et al. 2006, *MNRAS*, 365, 11, doi: [10.1111/j.1365-2966.2005.09675.x](https://doi.org/10.1111/j.1365-2966.2005.09675.x)
- De Lucia, G., & Blaizot, J. 2007, *MNRAS*, 375, 2, doi: [10.1111/j.1365-2966.2006.11287.x](https://doi.org/10.1111/j.1365-2966.2006.11287.x)
- Euclid Collaboration, Scaramella, R., Amiaux, J., et al. 2022, *A&A*, 662, A112, doi: [10.1051/0004-6361/202141938](https://doi.org/10.1051/0004-6361/202141938)
- Fang, Y., Hamaus, N., Jain, B., et al. 2019, *MNRAS*, 490, 3573, doi: [10.1093/mnras/stz2805](https://doi.org/10.1093/mnras/stz2805)

- Foreman-Mackey, D., Hogg, D. W., Lang, D., & Goodman, J. 2013, *PASP*, 125, 306, doi: [10.1086/670067](https://doi.org/10.1086/670067)
- Gong, Y., Liu, X., Cao, Y., et al. 2019, *ApJ*, 883, 203, doi: [10.3847/1538-4357/ab391e](https://doi.org/10.3847/1538-4357/ab391e)
- Guo, Q., White, S., Boylan-Kolchin, M., et al. 2011, *MNRAS*, 413, 101, doi: [10.1111/j.1365-2966.2010.18114.x](https://doi.org/10.1111/j.1365-2966.2010.18114.x)
- Hamaus, N., Sutter, P. M., & Wandelt, B. D. 2014a, *PhRvL*, 112, 251302, doi: [10.1103/PhysRevLett.112.251302](https://doi.org/10.1103/PhysRevLett.112.251302)
- Hamaus, N., Wandelt, B. D., Sutter, P. M., Lavaux, G., & Warren, M. S. 2014b, *PhRvL*, 112, 041304, doi: [10.1103/PhysRevLett.112.041304](https://doi.org/10.1103/PhysRevLett.112.041304)
- Henriques, B. M. B., White, S. D. M., Thomas, P. A., et al. 2015, *MNRAS*, 451, 2663, doi: [10.1093/mnras/stv705](https://doi.org/10.1093/mnras/stv705)
- Ivezić, Ž., Kahn, S. M., Tyson, J. A., et al. 2019, *ApJ*, 873, 111, doi: [10.3847/1538-4357/ab042c](https://doi.org/10.3847/1538-4357/ab042c)
- Kenneth E. Bellock. 2019, Alpha Shape Toolbox, <https://alphashape.readthedocs.io/en/latest/index.html>
- Lewis, A., Challinor, A., & Lasenby, A. 2000, *ApJ*, 538, 473, doi: [10.1086/309179](https://doi.org/10.1086/309179)
- Limber, D. N. 1954, *ApJ*, 119, 655, doi: [10.1086/145870](https://doi.org/10.1086/145870)
- Mauland, R., Elgarøy, Ø., Mota, D. F., & Winther, H. A. 2023, *A&A*, 674, A185, doi: [10.1051/0004-6361/202346287](https://doi.org/10.1051/0004-6361/202346287)
- Miao, H., Gong, Y., Chen, X., et al. 2023, *MNRAS*, 519, 1132, doi: [10.1093/mnras/stac3583](https://doi.org/10.1093/mnras/stac3583)
- Murray, S. G. 2018, *The Journal of Open Source Software*, 3, 850, doi: [10.21105/joss.00850](https://doi.org/10.21105/joss.00850)
- OpenCV. 2015, Open Source Computer Vision Library, <http://docs.opencv.org/>
- Pei, W., Guo, Q., Li, M., et al. 2024, *MNRAS*, 529, 4958, doi: [10.1093/mnras/stae866](https://doi.org/10.1093/mnras/stae866)
- Pellicciari, D., Contarini, S., Marulli, F., et al. 2023, *MNRAS*, 522, 152, doi: [10.1093/mnras/stad956](https://doi.org/10.1093/mnras/stad956)
- Planck Collaboration, Aghanim, N., Akrami, Y., et al. 2020, *A&A*, 641, A6, doi: [10.1051/0004-6361/201833910](https://doi.org/10.1051/0004-6361/201833910)
- Platen, E., van de Weygaert, R., & Jones, B. J. T. 2007, *MNRAS*, 380, 551, doi: [10.1111/j.1365-2966.2007.12125.x](https://doi.org/10.1111/j.1365-2966.2007.12125.x)
- Sánchez, C., Clampitt, J., Kovacs, A., et al. 2017, *MNRAS*, 465, 746, doi: [10.1093/mnras/stw2745](https://doi.org/10.1093/mnras/stw2745)
- Schuster, N., Hamaus, N., Dolag, K., & Weller, J. 2023, *JCAP*, 2023, 031, doi: [10.1088/1475-7516/2023/05/031](https://doi.org/10.1088/1475-7516/2023/05/031)
- Song, Y., Xiong, Q., Gong, Y., et al. 2024a, *MNRAS*, 532, 1049, doi: [10.1093/mnras/stae1575](https://doi.org/10.1093/mnras/stae1575)
- Song, Y., et al. 2024b, *MNRAS*, 534, 128, doi: [10.1093/mnras/stae2094](https://doi.org/10.1093/mnras/stae2094)
- Song, Y., Xiong, Q., Gong, Y., et al. 2024c, arXiv e-prints, arXiv:2408.08589. <https://arxiv.org/abs/2408.08589>
- Springel, V. 2005, *MNRAS*, 364, 1105, doi: [10.1111/j.1365-2966.2005.09655.x](https://doi.org/10.1111/j.1365-2966.2005.09655.x)
- Springel, V., Yoshida, N., & White, S. D. M. 2001, *NewA*, 6, 79, doi: [10.1016/S1384-1076\(01\)00042-2](https://doi.org/10.1016/S1384-1076(01)00042-2)
- van de Weygaert, R., & Schaap, W. 2009, in *Data Analysis in Cosmology*, ed. V. J. Martínez, E. Saar, E. Martínez-González, & M. J. Pons-Bordería, Vol. 665, 291–413, doi: [10.1007/978-3-540-44767-2_11](https://doi.org/10.1007/978-3-540-44767-2_11)
- Verza, G., Carbone, C., Pisani, A., Porciani, C., & Matarrese, S. 2024, arXiv e-prints, arXiv:2401.14451, doi: [10.48550/arXiv.2401.14451](https://doi.org/10.48550/arXiv.2401.14451)
- Vielzeuf, P., Calabrese, M., Carbone, C., Fabbian, G., & Baccigalupi, C. 2023, *JCAP*, 2023, 010, doi: [10.1088/1475-7516/2023/08/010](https://doi.org/10.1088/1475-7516/2023/08/010)
- Vielzeuf, P., Kovács, A., Demirbozan, U., et al. 2021, *MNRAS*, 500, 464, doi: [10.1093/mnras/staa3231](https://doi.org/10.1093/mnras/staa3231)
- Virtanen, P., Gommers, R., Oliphant, T. E., et al. 2020, *Nature Methods*, 17, 261, doi: [10.1038/s41592-019-0686-2](https://doi.org/10.1038/s41592-019-0686-2)
- Zhan, H. 2011, *Scientia Sinica Physica, Mechanica & Astronomica*, 41, 1441, doi: [10.1360/132011-961](https://doi.org/10.1360/132011-961)
- Zhan, H. 2021, *Chinese Science Bulletin*, 66, 1290, doi: [10.1360/TB-2021-0016](https://doi.org/10.1360/TB-2021-0016)